Pile driving induced vibrations: prediction based on a time-domain nonlinear hyperelastic model

Tales Vieira Sofiste[1], Luís Godinho[1], Pedro Alves Costa[2], Delfim Soares[3]

[1]University of Coimbra, ISISE, Department of Civil Engineering, Coimbra, Portugal
{tales.sofiste@uc.pt; lgodinho@dec.uc.pt}
[2]University of Porto, CONSTRUCT, Faculty of Engineering, Porto, Portugal
{pacosta@fe.up.pt}
[3]Federal University of Juiz de Fora, Department of Structural Engineering, Juiz de Fora, Brazil
{delfim.soares@ufjf.edu.br}

Abstract

Pile driving operation generates considerable disturbance to nearby buildings in terms of noise and vibrations. This study is focused on ground-borne vibrations, which are difficult to predict and mitigate. Several factors may influence the propagation pattern and intensity, which may even cause structural damage in extreme cases. In this sense, the correct prediction of the level of the vibrations prior to the pile driving operation is extremely important. In this work, an axisymmetric finite element model is implemented in time-domain, considering an efficient explicit/semi-explicit time marching procedure. The soil is modelled as a nonlinear elastic model, according to a classical hyperbolic model available in the literature. A numerical application is carried out and the obtained results are analyzed and compared to previous numerical and experimental studies.

Keywords: pile driving, ground-borne vibrations, finite element method, nonlinear analyses, time domain simulations.

1   Introduction

Linear analysis of ground-borne vibrations induced by pile driving are reasonably suitable when low strains are developed in the soil [1,2]. However, this is not the case when real scenarios are analyzed. In this type of operation, a large amount of energy is transmitted through the soil and considerable strains occur in the vicinity of the pile. As a consequence, the developed strains in this restricted area surpass the linear elastic range. In this work, these vibrations are studied considering a nonlinear behavior based on a hyperbolic model. The classical hyperbolic model proposed by Hardin and Drnevich [3] is employed and compared to previous numerical studies and field measurements available in the literature [1]. The finite element method (FEM) [4,5], a widely employed numerical tool, is adopted considering axisymmetric formulation for the discretization of the soil and pile, and the resulting equation of motion is solved in the time domain.

Time domain simulations stand as an efficient approach to deal with wave propagation problems. In the case of pile driving, the soil and site conditions may be simulated considering different geometric and physical properties and, for this reason, it presents technical advantages when compared to classical energy-based relations [6-8]. As it is well stablished, when implicit [9-10] methods are employed in nonlinear analyses, an iterative process takes place within each time step, which considerably increases the computational costs. Here, a semi-explicit/explicit time marching procedure proposed by Soares [11] is applied. The crucial advantage of this method for the present simulation is that local implicit subdomains may be applied without the need of iterative processes. Thus, implicit subdomains may be generated in restricted areas of the domain and, therefore, the problem may be partially solved as implicit and partially as explicit, considerably diminishing the computational efforts of the solution procedure.

2 Governing equations and time integration scheme

Considering the time domain FEM formulation, the equation of motion for a nonlinear system may be given by [12]:

$$\mathbf{M}\ddot{\mathbf{U}}(t) + \mathbf{C}\dot{\mathbf{U}}(t) + \mathbf{P}(t) = \mathbf{F}(t), \tag{1}$$

where $\mathbf{M}$ and $\mathbf{C}$ are the mass and damping matrices, respectively; $\ddot{\mathbf{U}}(t)$ and $\dot{\mathbf{U}}(t)$ are the accelerations and velocities vectors, respectively; and $\mathbf{F}(t)$ is the external forces vector. $\mathbf{P}(t)$ is the internal forces vector and it is defined as function of $\mathbf{U}(t)$, where $\mathbf{U}(t)$ is the displacement vector. In linear analyses, this vector may be defined as:

$$\mathbf{P}(t) = \mathbf{K}\mathbf{U}(t), \tag{2}$$

where $\mathbf{K}$ stands for the stifness matrix. In this work, since explicit nonlinear analyses are regarded, the internal forces vector is computed at each time step according to the previously obtained response. The initial conditions of this system are given by: $\mathbf{U}(0) = \mathbf{U}^0$ and $\dot{\mathbf{U}}(0) = \dot{\mathbf{U}}^0$ ($\mathbf{U}^0$ stands for the initial displacement vector and $\dot{\mathbf{U}}^0$ stands for the initial velocity vector). The equation of motion (Equation 1) is solved in the time domain taking into account the semi-explicit/explicit time marching procedure proposed by Soares [11]. This time integration scheme is defined with the same approximations to the time derivatives of the displacement field as in the standard Central Difference Method (CDM), which are given by:

$$\ddot{\mathbf{U}}^n = \frac{1}{\Delta t^2}(\mathbf{U}^{n+1} - 2\mathbf{U}^n + \mathbf{U}^{n-1}), \tag{3}$$

$$\dot{\mathbf{U}}^n = \frac{1}{2\Delta t}(\mathbf{U}^{n+1} - \mathbf{U}^{n-1}), \tag{4}$$

where the superscript "n" indicates the time step of the variable and $t = n\Delta t$. The recursive relation proposed by Soares [11] is given by:

$$\left(\overline{\mathbf{M}}_e + \frac{1}{2}\Delta t \mathbf{C}_e\right)\mathbf{U}_e^{n+1} = \Delta t^2(\mathbf{F}_e^n - \mathbf{P}_e^n) + \overline{\mathbf{M}}_e(2\mathbf{U}_e^n - \mathbf{U}_e^{n-1}) + \frac{1}{2}\Delta t \mathbf{C}_e \mathbf{U}_e^{n-1}, \tag{5}$$

where the subscript "e" indicates that the variable is locally defined (i.e., it is defined at an element level). $\overline{\mathbf{M}}_e$ stands for the modified local matrix, and the standard Central Difference Method is reproduced when $\overline{\mathbf{M}}_e = \mathbf{M}_e$ is considered. This modified matrix is defined in order to ensure the stability of the method. As it is well known, CDM is a classical conditionally stable explicit method, with critical sampling frequency $\Omega_c = 2$. Thus, the method proposed by Soares [11] is defined so that the mass matrix is locally modified whenever it is necessary (i.e., when an explicit element is unstable, its local mass matrix is modified and an implicit stable element is then generated). The modified local matrix is defined as:

$$\overline{\mathbf{M}}_e = \mathbf{M}_e + \Delta t^2 a_e \mathbf{K}_e, \tag{6}$$

where a_e is a local parameter that defines the explicit and implicit subdomains. Thus, the maximum critical sampling frequency of the element is evaluated and, if it is greater than 2 (unstable element), a proper non-null value is defined to the parameter a_e and stability is ensured. This parameter is given by:

$$\text{if } \Omega_e^{max} \le 2, a_e = 0, \tag{7}$$

$$\text{if } \Omega_e^{max} > 2, a_e = \frac{1}{4}\tanh\left(\frac{1}{4}\Omega_e^{max}\right), \tag{8}$$

where Ω_e^{max} stands for the maximum sampling frequency of the element. Hence, the classical explicit CDM is reproduced whenever the element is stable ($\Omega_e^{max} \leq 2$) and a novel implicit method arises when the element is unstable ($\Omega_e^{max} > 2$). For simplicity, in this work, the parameter a_e regarding the generation of implicit subdomains is considered as:

$$\text{if } \Omega_e^{max} > 2, a_e = \frac{1}{4}, \tag{9}$$

which allows to enhance the stability of the model. The variable Ω_e^{max} is given by:

$$\Omega_e^{max} = \omega_e^{max}\Delta t, \tag{10}$$

where ω_e is the maximum natural frequency of the element, which is calculated as the square root of the maximum eigenvalue of the locally defined generalized eigenvalue problem [4,5]:

$$\mathbf{K}_e\phi_e = \omega_e^2\mathbf{M}_e\phi_e. \tag{11}$$

The innovative time integration scheme proposed by Soares [11] is simple to implement and entirely automated, since the user must only define the time step of the analysis. Thus, explicit and implicit subdomains are automatically generated according to the geometrical and physical properties of each finite element. For further insights regarding this method, see [11].

3   Hyperelastic model

In this work, the classical hyperelastic model proposed by Hardin and Drnevich [3] is adopted. This model is simple to implement in numerical analyses and is widely used in soil dynamics. The stress-strain relation of this method is presented in Figure 1.
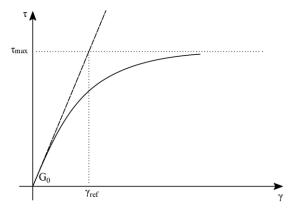

Figure 1 – Stress-strain relation of the Hardin and Drnevich model.

In terms of the shear modulus reduction factor, the Hardin and Drnevich model is defined as [3]:

$$\frac{G_s}{G_0} = \frac{1}{1+\frac{\gamma}{\gamma_{ref}}}, \tag{12}$$

where G_s is the secant shear modulus, G_0 is the initial shear modulus (corresponding to linear elastic behavior), γ is the shear strain and γ_{ref} is the reference strain.

4 Implemented model

4.1 Model dimensions and properties

The parametric study published by Masoumi et al. [1] is reproduced here. Three pile penetration depths are analyzed: $h_1 = 2\,[m]$, $h_2 = 5\,[m]$ and $h_3 = 10\,[m]$. The FEM axisymmetric formulation is adopted, considering linear triangular elements (3 nodes). A sketch of the implemented model for the penetration depth $h_3 = 10\,[m]$ is presented in Figure 2.
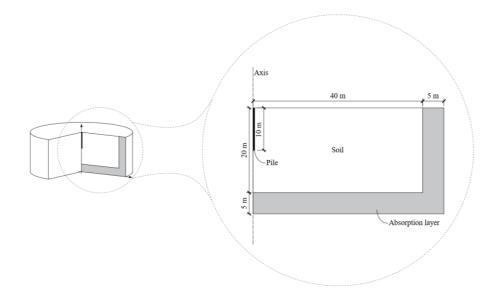

Figure 2 – Sketch of the numerical model for the penetration depth $h_3 = 10\,[m]$ considering axisymmetric formulation.

The model dimensions are: $H_{soil} = 20\,[m]$ (soil depth), $L_{soil} = 40\,[m]$ (soil length). An absorption layer is also modelled, with $l_{damp} = 5\,[m]$ to damp out reflections on the boundary of the domain and simulate an infinite medium (the material damping formulation is further explained in Section 4.3). A concrete pile with circular cross section is adopted with $L_{pile} = 10\,[m]$ (pile length), $d_{pile} = 0.50\,[m]$ (pile diameter), $E_{pile} = 40\,GPa$ (Young modulus), $v_{pile} = 0.25\,[-]$ (Poisson ratio) and $\rho_{pile} = 2500\,[kg/m^3]$ (mass density). The pile is modeled as linear elastic and two scenarios are considered for the soil behavior: linear and nonlinear elastic. Soil properties for the implemented scenarios are presented in Table 1. The nonlinear property γ_{ref} is based on "Table 5 – Tests on Leek Creek Silt" presented by Hardin and Drnevich [3]. For the analyzed soil, the stress-strain relation and the equivalent linear shear modulus reduction are presented in Figure 3.

Table 1 – Studied soil scenarios.

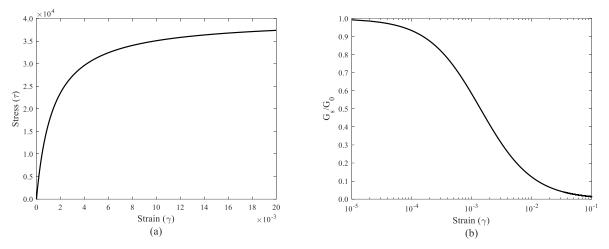| Scenario	1	2
Soil behavior	Linear	Nonlinear
Hyperbolic model	-	Hardin and Drnevich
Young modulus	$E_{soil} = 80\,[MPa]$	$E_{soil} = 80\,[MPa]$
Shear modulus	$G_{soil} = 28.5\,MPa]$	$G_{soil} = 28.5\,[MPa]$
Poison ratio	$v_{soil} = 0.40\,[-]$	$v_{soil} = 0.40\,[-]$
Mass density	$\rho_{soil} = 2000\,[kg/m^3]$	$\rho_{soil} = 2000\,[kg/m^3]$
Model parameters	-	$\gamma_{ref} = 1.4 \times 10^{-3}\,[-]$

Figure 3 – Soil properties: (a) Stress-strain relation and (b) Shear modulus reduction with strain.

4.2   Implicit and explicit subdomains decomposition

The finite element mesh adopted in the numerical application is generated in *Gmsh* [13]. A mesh refinement is considered in order to obtain a better result near the pile, where the nonlinear behavior is expected to occur, due to the higher magnitude of the developed strains. A sketch of the mesh refinement for the penetration depth $h_3 = 10\,[m]$ is presented in Figure 4 (the hatched area near the pile is considered with elements twice smaller than the rest).
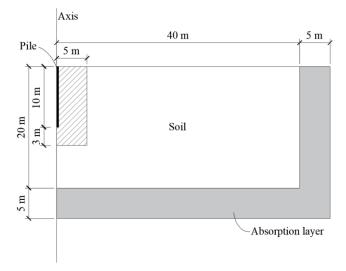

Figure 4 – Sketch of the adopted mesh refinement (hatched area) for the penetration depth $h_3 = 10\,[m]$.

The dimensions $h_{ref} = 3\,[m]$ (from the pile toe) and $d_{ref} = 5\,[m]$ (from the pile axis) for the mesh refinement are also adopted for the penetration depths $h_1 = 2\,[m]$ and $h_2 = 5\,[m]$. Thus, the number of elements is different according to the penetration depth, as presented in Table 2.

Table 2 – Number of nodes and elements of the adopted meshes.

Penetration depth	Nodes	Elements
$h_1 = 2\,[m]$	7230	14081
$h_2 = 5\,[m]$	7674	14989
$h_3 = 10\,[m]$	7952	15579

As previously described in Section 2, the method proposed by Soares [11] automatically generate implicit and explicit subdomains according to the properties of the finite element. Hence, the time-step of the analysis is selected in a way that the pile and the refined area (see Figure 4) is stablished as an implicit subdomain, in order to ensure the stability of the model. For this model properties and dimensions, the critical time-step is $\Delta t_{crit} = 1.78 \times 10^{-5} \, [s]$ for a purely explicit analysis and the adopted time step is $\Delta t = 2 \times 10^{-4} \, [s]$.

4.3 Material damping approach

The material damping approach adopted in this work is based on a previous study published by the authors [2]. The pile, computed as an implicit subdomain, is considered as Rayleigh damping:

$$\mathbf{C} = \alpha_{pile}\mathbf{M} + \beta_{pile}\mathbf{K}, \tag{13}$$

where α_{pile} and β_{pile} are defined as:

$$\alpha_{pile} = \frac{2\xi_{pile}\omega_{pile}^i\omega_{pile}^j}{\omega_{pile}^i+\omega_{pile}^j}, \tag{14}$$

$$\beta_{pile} = \frac{2\xi_{pile}}{\omega_{pile}^i+\omega_{pile}^j} \tag{15}$$

where ω_{pile}^i and ω_{pile}^j stand for the control frequencies of the Rayleigh damping and ξ_{pile} stand for the damping ratio of the pile ($\xi_{pile} = 2.5\%$). These control frequencies are selected as the first and third natural frequencies corresponding to axial vibration modes of the pile, which corresponds to $\omega_{pile}^i = 200 \, [Hz]$ and $\omega_{pile}^j = 600 \, [Hz]$. The material damping approach considered for the soil is different for the implicit and explicit subdomains. In the implicit domain (refined mesh area) of the soil, the damping matrix is considered as non-diagonal Rayleigh damping, given by:

$$\mathbf{C} = \alpha_{soil}\mathbf{M} + \beta_{soil}\mathbf{K}, \tag{16}$$

where α_{soil} and β_{soil} are defined as [2]:

$$\alpha_{soil} = \frac{2\omega_{soil}^i\omega_{soil}^j\left(\omega_{soil}^j\xi_{soil}^i-\omega_{soil}^i\xi_{soil}^j\right)}{\left(\omega_{soil}^j\right)^2-\left(\omega_{soil}^i\right)^2}, \tag{17}$$

$$\beta_{soil} = \frac{2\left(\omega_{soil}^j\xi_{soil}^j-\omega_{soil}^i\xi_{soil}^i\right)}{\left(\omega_{soil}^j\right)^2-\left(\omega_{soil}^i\right)^2}, \tag{18}$$

where ω_{soil}^i and ω_{soil}^j stand for the control frequencies of the Rayleigh damping and ξ_{soil}^i and ξ_{soil}^j stand for the selected damping ratios. In this work, it is adopted $\omega_{soil}^i = 10 \, [Hz]$, $\omega_{soil}^j = 200 \, [Hz]$, $\xi_{soil}^i = 1\%$ and $\xi_{soil}^j = 2\%$ (properties extracted from [2]). For the explicit subdomain, the modified local mass proportional damping proposed by [2] is considered:

$$\mathbf{C}_e = \left(\alpha_{soil} + \beta_{soil}\omega_e^{max}\left(\frac{\omega_{soil}^i\omega_{soil}^j}{\omega_{soil}^i+\omega_{soil}^j}\right)\right)\mathbf{M}_e, \tag{19}$$

where α_{soil}, β_{soil}, ω_{soil}^i and ω_{soil}^j are the same as described in Equations 17 and 18; and ω_e^{max} stands for the maximum natural frequency of the element, defined in Equation 11. For the damping layer, the material

damping is computed taking into account the Equation 19 and considering an exponential increasing of the damping ratio up to its exterior boundary. In addition, no numerical damping is adopted in this work, since stiffness proportional damping is considered and this approach presents strong dissipation of the higher frequencies.

5   Numerical application

5.1   Hammer impact force

Ground-borne vibrations induced by impact pile driving are studied here. In order to obtain the impact force, the hammer is considered according to a two degrees of freedom model proposed by Deeks and Randolph [14]. The hammer properties are extracted from Masoumi [1] and two impact scenarios are analyzed: a lower impact force with transmitted energy of approximately $E_t^{low} = 3.4\ [kJ]$ and a upper impact force with approximately $E_t^{up} = 19.2\ [kJ]$. Thus, for each scenario, a single blow of a BSP-357 hammer impact force (Figure 5) is applied in the center of the pile head.
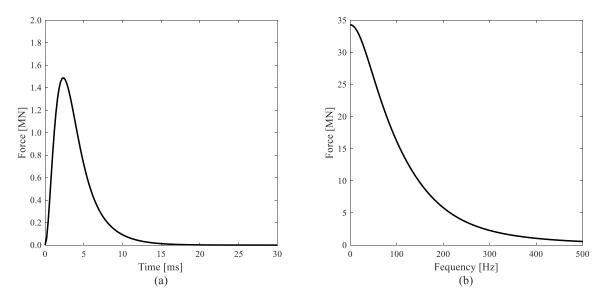

Figure 6 – Lower impact force: (a) time domain and (b) frequency domain.

5.2   Results and discussion

Figure 7 presents snapshots for the wave propagation (norm of the displacement), for the penetration depth $h_3 = 10\ [m]$ and for the linear and nonlinear analyses, considering the upper impact force. Here, the damping layers are not depicted in the snapshots, but it may be observed that they are working as expected (i.e., no spurious reflections are observed). The separation of different types of waves generated are also observed, since surface waves and body waves present slightly different propagation velocities. In addition, it is also observed the effect of the nonlinearity in the propagation pattern. The snapshots related to the linear behavior of the soil (Figure 7(a)) present higher energy than those related to the nonlinear model (Figure 7(b)).

Time history and frequency content for a surface point located at a radial distance $r = 5\ [m]$ from the center of the pile, considering a lower impact force, is presented in Figure 8. The effect of the nonlinear behavior of the soil is smaller when lower impact energies are applied. In fact, a smaller amount of energy induces a smaller magnitude of the developed strains which leads to a smoother nonlinearity. Still, the degradation of the shear modulus due to the nonlinear behavior may be observed in the propagation velocity of the surface waves, even for the lower impact force. As one may observe, results obtained in the nonlinear analysis present a latter arrival of the wave front.
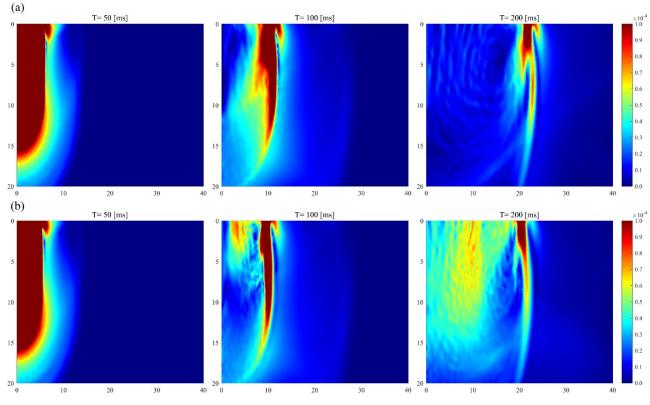
Figure 7 – Snapshots of the norm of the displacement: (a) linear and (b) nonlinear.
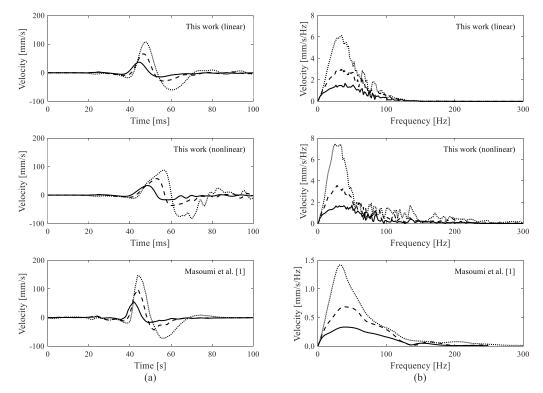

Figure 8 – Vertical velocity for a surface point located at radial distance $r = 5$ $[m]$: (a) time domain and (b) frequency domain for penetration depths $h_1 = 2$ $[m]$ (dotted line), $h_2 = 5$ $[m]$ (dashed line) and $h_3 = 10$ $[m]$ (solid line).

8

In Figure 9 the peak particle envelope for linear and nonlinear analyses are presented. The upper limit of the envelope corresponds to the upper impact force ($E_t^{up} = 19.2 \, [kJ]$) for the penetration depth $h_1 = 2 \, [m]$. On the other hand, the lower limit of this envelope corresponds to the lower impact force ($E_t^{low} = 3.4 \, [kJ]$) for the penetration depth $h_3 = 10 \, [m]$. Here, the effect of the nonlinearity of the soil is clearly observed. For the case of nonlinear analysis, a considerable amount of energy is internally dissipated. A substantial difference is shown for higher impact forces since then the developed strains reach higher magnitudes, resulting in a stronger nonlinear behavior.
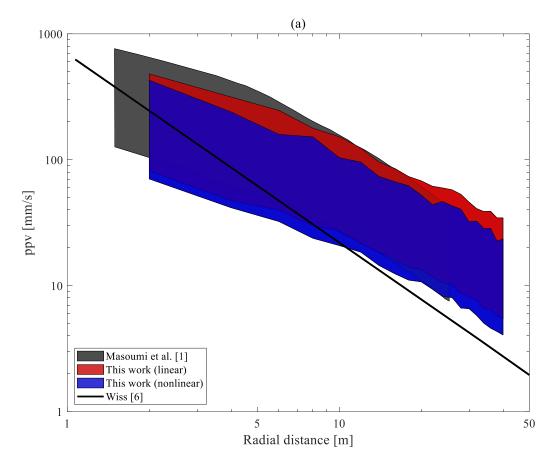

Figure 9 – Peak particle velocity envelope.

6 Conclusions

In this work a nonlinear numerical model is developed taking into account an effective time marching procedure. The adopted scheme allowed to implement implicit and explicit subdomains in the same analysis, without the need of iterative processes for solving the equation of motion. The obtained results are compared to previous numerical and field measurements, which are available in the literature. In order to obtain a comparable reference, a linear model with the same characteristics is also considered. The results demonstrate that a considerable amount of energy is dissipated due to the nonlinear behavior of the soil. In fact, pile driving operation induces significant strains in the vicinity of the pile and the adoption of a linear elastic constitutive behavior is not feasible when higher impact energy is considered. In addition, the results showed that the greater the impact force, the more energy is dissipated due to the nonlinearity behavior. Finally, important aspects of the wave propagation are properly observed, such as the influence of the pile penetration depth and the separation between different types of waves generated during the pile driving operation.

Acknowledgements

References

[1] Masoumi, H.R.; Degrande, G.; Lombaert, G. Prediction of free field vibrations due to pile driving using a dynamic soil-structure interaction formulation. *Soil Dynamics and Earthquake Engineering*, Vol. 27(2), 2007, pp. 126-143.

[2] Sofiste, T.V.; Godinho, L.; Costa, P.A.; Soares, D.; Colaço, A. Numerical modelling for prediction of ground-borne vibrations induced by pile driving. *Engineering Structures*, Vol. 242, 2021, pp. 112533.

[3] Hardin, B.O.; Drnevich, V.P. Shear modulus and damping in soils: design equations and curves. *Journal of the Soil mechanics and Foundations Division*, Vol 98(7), 1972, pp. 667-692.

[4] Bathe, K.J. *Finite Element Procedures* (2nd Edition), Klaus-Jürgen Bathe, Watertown - MA, 2014.

[5] Zienkiewicz, O.C.; Taylor, R.L.; Zhu, J.Z. *The Finite Element Method: Its Basis and Fundamentals* (6th Edition), Butterworth-Heinemann, Oxford, 2005.

[6] Wiss, J.F. Construction vibrations: state-of-the-art. *Journal of Geotechnical and Geoenvironmental Engineering*, Vol. 107, 1981, pp. 167-181.

[7] Attewell P.B.; Farmer I.W. Attenuation of ground vibrations from pile driving. *Ground Engineeering*, Vol 6(4), 1973, pp. 26-9.

[8] Attewell P.B.; Selby A.R.; O'Donnell L. Estimation of ground vibration from driven piling based on statistical analyses of recorded data. *Geotechnical & Geological Engineering*, Vol 10, 1992, pp. 41–59.

[9] Newmark, N. M. A method of computation for structural dynamics. *Journal of the Engineering Mechanics Division*, Vol. 85(3), 1959, pp. 67-94.

[10] Hilber, H. M.; Hughes, T. J.; Taylor, R. L. Improved numerical dissipation for time integration algorithms in structural dynamics. *Earthquake Engineering & Structural Dynamics*, Vol. 5(3), 1977, pp. 283-292.

[11] Soares Jr, D. An adaptive semi-explicit/explicit time marching technique for nonlinear dynamics. *Computer Methods in Applied Mechanics and Engineering*, Vol. 354, 2019, pp. 637-662.

[12] Clough, R.W.; Penzien, J. *Dynamics of Structures*, Computers & Structures, Inc, Berkeley - CA, 1995.

[13] Geuzaine, C.; Remacle, J. F. Gmsh: A 3-D finite element mesh generator with built-in pre-and post-processing facilities. *International Journal for Numerical Methods in Engineering*, Vol. 79(11), 2009, pp. 1309-1331.

[14] Deeks, A. J.; Randolph, M. F. Analytical modelling of hammer impact for pile driving. *International Journal for Numerical and Analytical Methods in Geomechanics*, Vol. 17(5), 1993, pp. 279-302.